Response of an Urban Bus Flywheel Battery to a Rapid Loss-of-Vacuum Event

R.C. Thompson
The University of Texas at Austin Center for Electromechanics

J. Kramer
Argonne National Laboratory (current address: Winter Park, CO)

R.J. Hayes
The University of Texas at Austin Center for Electromechanics

.

ABSTRACT

The University of Texas at Austin Center for Electromechanics (UT-CEM) is developing a 2 kW-hr flywheel battery for energy management on a hybrid electric urban bus. The battery will recover braking energy and store excess energy generated by the prime mover. The flywheel rotor, fabricated from high-strength composites, spins at 40,000 rpm at full charge (~900 m/s tip speed), and is housed in a vacuum enclosure to minimize windage drag. Also integrated into the enclosure is a composite containment system that has been proof-tested to provide additional safety.

Ensuring flywheel safety is a major issue that must be addressed in using flywheels for transportation applications. A large leak caused by a service failure of the vacuum system could damage the flywheel before the energy dump system has time to act.

A rapid loss-of-vacuum test on a rotor similar to that planned for the urban bus flywheel was conducted. Instrumentation, during the flywheel spin test recorded increasing flywheel surface temperature (>316°C or 600°F) following an intentional and abrupt loss of vacuum. No severe damage was noted on the surface of the flywheel, which was later retested to a higher speed to assess structural integrity. This paper provides an analysis of the data from that test and discusses the experimental results as they pertain to safety of the bus flywheel.

INTRODUCTION

The University of Texas Center for Electromechanics (UT-CEM) has developed a 2 kW-hr flywheel battery for energy management on a hybrid electric bus; and, successfully commissioned on the bus in September 2002. The battery stores braking energy and excess energy generated by the prime mover (e.g., internal combustion engine) for recovery during peak demand situations. The flywheel rotor is fabricated from high strength carbon fiber composite and spins at 40,000 rpm at full charge. The tip speed of the rotor at this angular velocity is in excess of 900 m/s. Consequently, the rotor must be housed in a vacuum enclosure to minimize the power loss from windage drag and to prevent drag forces from overheating the composite. The flywheel is housed inside a composite containment system. This containment system design has been proven through flywheel burst tests and provides additional safety.

Flywheel safety is a major concern that must be addressed in using flywheels for transportation applications. Argonne National Laboratory has performed a preliminary safety assessment of the urban bus system in which several accident initiators were identified for consideration. Among these initiators were slow loss-of-vacuum and rapid loss-of-vacuum events, the two being distinguished by the time for pressurization of the containment compared to the time for the energy dump system on the bus to effectively de-energize the flywheel.

The energy dump system was designed to use the dynamic braking resistor, which is normally used to augment the pneumatic or electric wheel brakes. The dynamic braking system functions by operating the traction motors as generators in order to convert the bus kinetic energy to braking energy, which is then dissipated as heat in an air-cooled resistor grid. The dynamic brake resistor can also function as a flywheel energy dump resistor during emergency situations. Under these conditions the dump system is capable of removing 150 kW at 40,000 rpm. The converter for the flywheel motor/generator is designed to maintain nearly constant braking torque as the flywheel slows. Consequently, the flywheel angular velocity and power decrease nearly linearly with time. Integration of the power over the energy dump sequence shows that the time to spin down to zero velocity is approximately equal to the initial stored energy (2 kW-hr) divided by half the initial power (150 kW), or about 100 s. Thus, any containment pressurization event that occurs more rapidly than 100 s is considered here to be a rapid loss-of-vacuum event and any containment pressurization event that occurs more slowly than 100 s is considered to be a slow loss-of-vacuum event.

The two major sources for a loss of vacuum are loss of the vacuum pump or leaks in the flywheel housing or vacuum lines. Loss of the vacuum pump through either a mechanical or electrical failure is likely to constitute a slow loss-of-vacuum event because the only source of pressurization is through normal seal leakage or out-gassing of the flywheel, both of which are very slow processes on the time scale of 100 s or more. Similarly, small leaks in the containment or the vacuum line can be accommodated by the vacuum pump. Once failures in the vacuum system are detected, the flywheel can be de-energized before it heats up sufficiently to cause a concern. On the other hand, a large leak caused by a service failure of the vacuum system (such as fatigue failure of a weld or a breach caused by a bus crash) could damage the flywheel before the dump system has time to act. The calculations given in Appendix A of this study suggest a critical effective leak diameter of 0.1 mm. Any larger leak would be sufficient to pressurize the free volume inside the bus flywheel vacuum enclosure in less than 100 s.

One of the conclusions of the preliminary safety report [1] was that, of the accident initiators studied, the rapid loss-of-vacuum event had the highest probability of leading to flywheel damage sufficient to challenge the containment. This conclusion was based on calculations which showed that the flywheel surface temperatures could exceed the glass transition temperature of the resin during this event. Since it was unknown at the time what the consequences of this overheating would be, it was necessary to assume the worst: all material that exceeded the glass transition temperature was assumed to fail in a way that would lead to the greatest rotor imbalance, i.e. over a 180° sector. If this were the case, the shaking forces would probably be sufficient to break the rotor loose, which (because of a lack of sufficient experimental evidence) was judged to constitute a challenge to the containment integrity. One of the recommendations in the report was to conduct a rapid loss-of-vacuum test on the flywheel rotor so that the conservatism in the analysis could be removed.

A rapid loss-of-vacuum test on a rotor similar to that planned for the urban bus flywheel was conducted by UT-CEM at Test Devices, Inc. in February, 1998. The present paper provides an analysis of the data from that test and discusses the experimental results in light of the safety of the bus flywheel.

COMPOSITE FLYWHEEL DESIGN AND FABRICATION PROCESS

Flywheel's energy storage potential is proportional to its mass polar moment of inertia and the square of the rotational speed. Specific energy (stored kinetic energy/system mass) is limited by the material's strength-to-density ratio, and for this reason, high strength composite materials are the preferred flywheel material. The flywheel topology for the hybrid electric bus is a preloaded design; and is assembled from eight individual rings fabricated from carbon fiber tow impregnated with a toughened epoxy. All composite rings are assembled by interference fit which preloads the rings and maintains a radial compressive stress state at all speeds, thereby preventing delaminations which lead to mass balance perturbations. A solid metallic hub or shaft serves as the foundation of the preloaded flywheel design. Preloaded composite flywheels are robust structures, with excellent mass balance stability and high torque capacity.

The composite flywheel rings were fabricated using impregnated tow (towpreg) using a toughened resin system. Off-axis fiber reinforcement is included to add fracture toughness to the laminate and prevent/mitigate the formation of cracks. This fabrication process is autoclave based, to assist with consolidation and to reduce void content. Hexcel's recommended 8552 cure cycle was used for the autoclave processing. The 12K towpreg consisted of Hexcel's IM7 fiber and Hexcel's 8552 resin with a resin content of about 33%.

The flywheel's design factor of safety is about 1.5, but for additional safety, the composite containment system was added.

TEST DESCRIPTION

The UT-CEM loss-of-vacuum test used a flywheel that had been used previously for other testing. The rotor design and dimensions were similar to those for the urban bus flywheel battery; however, the test was on a "bare" rotor conducted inside of a spin pit without a prototypical containment. The test configuration is shown in Fig. 1. Table 1 compares the gap dimensions in the test with the anticipated close-fitting containment dimensions for the bus flywheel battery system.

The loss-of-vacuum test was conducted inside the 48 in. spin pit at Test Devices, Inc. in Hudson, Massachusetts. The pit was initially evacuated to 100 mTorr and the rotor spun up to a speed of 40,625 rpm (outer rim tip speed of 925 m/s) using a quill shaft attached to an air turbine.

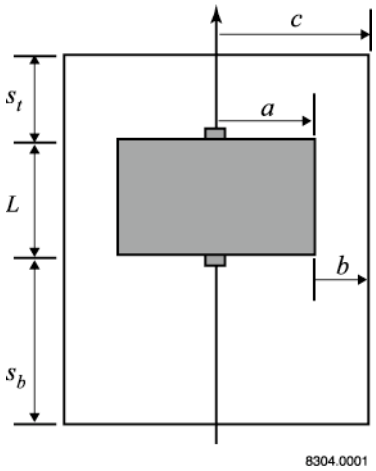

Fig. 1 Flywheel and containment geometry

Table 1. Flywheel and containment parameters for test conditions and battery design

	Symbol in Fig. 1	Test Geometry	Battery Geometry
Flywheel radius	a	8.56 in. (0.217 m)	8.75 in. (0.222 m)
Flywheel length	L	4.0 in. (0.102 m)	5.0 in. (0.127 m)
Radial gap	b	15.4 in. (0.392 m)	0.10 in. (2.54 mm)
Top axial gap	s_t	5.0 in. (0.127 m)	1.0 in. (25.4 mm)
Bottom axial gap	s_b	26.0 in. (0.660 m)	1.0 in. (25.4 mm)

After steady-state conditions were reached, the power to the turbine was cut off and the pit was rapidly pressurized with nitrogen to one atmosphere. The trace of the pit pressure vs. time showed that the pressurization was accomplished in less than 1 s, which was within the test specifications. Nitrogen was used in place of air for safety purposes.

Following pressurization, the rotor was allowed to spin down under the windage torque. The most relevant measurements during this period were the rotor speed as a function of time and the rotor surface temperature, which was measured with two calibrated infrared probes. A minor amount of fiber slinging was observed during the transient, but the rotor remained balanced and came to rest with the rotor and quill shaft intact. Inspection of the rotor following the test showed no obvious signs of damage, although it was warm to the touch.

Additional inspection was performed after the rotor was removed from the spin pit. Beyond the minor fiber sling mentioned above, no additional damage could be identified. The rotor was rebalanced, requiring only a slight mass balance correction to account for the lost material from the outer surface of the flywheel. The rotor was then placed back in the spin pit facility and spun to 46,600 rpm (outer rim tip speed of 1,060 m/s), failing the outer ring of the flywheel.

Circumferential tensile strain in the outer ring's composite laminate, at the flywheel's operational speed of 40,000 rpm, is about 1%. From hydroburst tests, the laminate's ultimate tensile strain is 1.5%, which equates to a shaft speed of xxxxx rpm. The fact that the flywheel during re-test, failed at 15% over the initial test speed (which was similar to the operating speed for the urban transit bus system) suggests that the transient elevated temperatures from the loss-of-vacuum event did degrade the structural integrity of the flywheel, but possessed sufficiently residual strength to avoid a catastrophic failure.

This test showed that one loss-of-vacuum occurrence is survivable. However, in practice, that flywheel would be removed from bus service and replaced with a new unit.

FLYWHEEL DRAG FORCES

Flywheel drag forces under the loss-of-vacuum conditions of interest here can be calculated using correlations that have been developed to compute the windage losses in rotating machinery. A review of the many studies that have been conducted in this area is provided in reference [2]. The correlations are generally presented in the form of a non-dimensional moment coefficient that is a function of Reynolds number and a non-dimensional gap parameter; however, most of the correlations have been developed for the two geometric

extremes of an infinitely long cylinder and a thin disk. Application of the correlations to a finite rotor requires the assumption that the overall torque on the rotor can be determined by applying the thin disk correlations to the end faces and the infinite cylinder correlations to the cylindrical face.

The most complete prescription for calculating drag forces on rotating machinery is contained in reference [3]. Recently, the correlations recommended in this reference have been applied successfully to the analysis of flywheel windage losses under normal operating conditions [4]. Because of this, the same correlations are used here to analyze the sudden loss-of-vacuum event. The notation that will be used is also the same as that used in the two references.

The disk torque coefficient C_m is defined such that the torque M_1 on one side of the disk is given by

$$M_1 = C_m \frac{\rho}{2} \omega^2 a^2 \qquad (1)$$

where ρ is the fluid density, a is the disk radius and ω is the angular velocity. Similarly, the cylinder torque coefficient C_f is defined such that the torque M_2 on the cylindrical face is given by

$$M_2 = C_f \pi a^4 L \rho \omega^2 \qquad (2)$$

where L is the length of the cylinder. A dimensional analysis of the governing equations shows that the torque coefficients are expected to be a function of the Reynolds number N_{Re} and the dimensionless gap, either s/a for the disk or b/a for the cylinder. The definitions of the gap dimensions are shown in figure 1 and the Reynolds number is defined by

$$N_{\mathrm{Re}} = \frac{\rho \omega a^2}{\mu} \qquad (3)$$

where μ is the dynamic viscosity. At the beginning of the spin down phase in the loss-of-vacuum test geometry, the Reynolds number is 1.3×10^7. Thus, initially, the flow is highly turbulent. As the flywheel velocity decreases, the flow crosses into a transition regime and, at very low speeds, becomes laminar. It is assumed here that the flow always remains quasi-static such that the drag at any speed is the same as that which would occur if the flywheel had been spinning under steady state conditions at that speed. In other words, the adjustments to the flow field are assumed to occur faster than the speed changes. Since the loss-of-vacuum test showed that the entire transient takes about 300 s, this assumption is reasonable. The only exception is near the beginning of the transient where the gas near the rotor surface must accelerate rapidly from zero velocity to the flywheel tip velocity of 925 m/s.

The drag correlations given in reference [3] are divided into two categories: one is for "unenclosed" rotors and the other is for "enclosed" rotors. Test data for unenclosed rotors were obtained under conditions where the containment diameter was much larger than the rotor diameter. The diameter ratio for the present loss-of-vacuum test conditions is approximately 2.8, according to Table 1. On the other hand, the ratio for the bus flywheel battery is approximately 1.01. Thus, it is reasonable to apply the correlations for unenclosed rotors to the test data, but to apply the correlations for an enclosed rotor to the battery design geometry. A comparison of the response of the rotor to these two conditions is given at the end of this section of the paper.

Correlations for the properties of both nitrogen and air are also given in [3]. Consistent with kinetic theory predictions, the viscosity, thermal conductivity and heat capacity are only functions of temperature for pressures between 100 mTorr and one atmosphere (760 Torr). The density is, of course, a strong function of both temperature and pressure. Here the ideal gas law has been used to model the pressure and temperature dependence of the density, with the density at 298 °K and one atmosphere obtained from the correlation given in [3]. Furthermore, the mean free path for nitrogen between 100 mTorr and one atmosphere ranges from 45 mm to 6×10^{-5} mm [5]. This implies that continuum models for the flow are applicable for all regimes of interest in the test geometry. The continuum model and related drag coefficients are probably not applicable under normal operating conditions in the flywheel battery design since the mean free path of the gas molecules is greater than the gap width between the rotor and the vacuum containment.

The torque coefficient [3] on the end faces of the "unenclosed" flywheel are divided into three flow regimes:

Laminar $N_{\mathrm{Re}} < 310{,}000$

$$C_m = \frac{1.9352}{\sqrt{N_{\mathrm{Re}}}} \qquad (4a)$$

Transition $310{,}000 < N_{\mathrm{Re}} < 7 \times 10^6$

$$C_m = \frac{0.073}{N_{\mathrm{Re}}^{0.2}} \qquad (4b)$$

Turbulent $N_{\mathrm{Re}} > 7 \times 10^6$

$$C_m = 0.491 \left[\log\left(N_{\mathrm{Re}}\right)\right]^{-2.58} \qquad (4c)$$

Similarly, the torque coefficient [3] on the cylindrical face of the rotor is given by

Laminar $N_{\mathrm{Re}} < 9.44$

$$C_f = \frac{4}{N_{\mathrm{Re}}} \tag{5a}$$

Transition $9.44 < N_{\mathrm{Re}} < 351$

$$\frac{1}{\sqrt{C_f}} = -1.76 + 4.07 \log\left(N_{\mathrm{Re}} \sqrt{C_f}\right) \tag{5b}$$

Turbulent $N_{\mathrm{Re}} > 351$

$$\frac{1}{\sqrt{C_f}} = -0.6 + 4.07 \log\left(N_{\mathrm{Re}} \sqrt{C_f}\right) \tag{5c}$$

The usual method of presenting the drag coefficients is to plot them versus Reynolds number. However, it is more instructive here to plot them as a function of the angular velocity during the rotor spin down, as shown in figures 2 and 3. The three regions in Eq. 4 and 5 are indicated in the figures by A-B (laminar), B-C (transition) and C-D

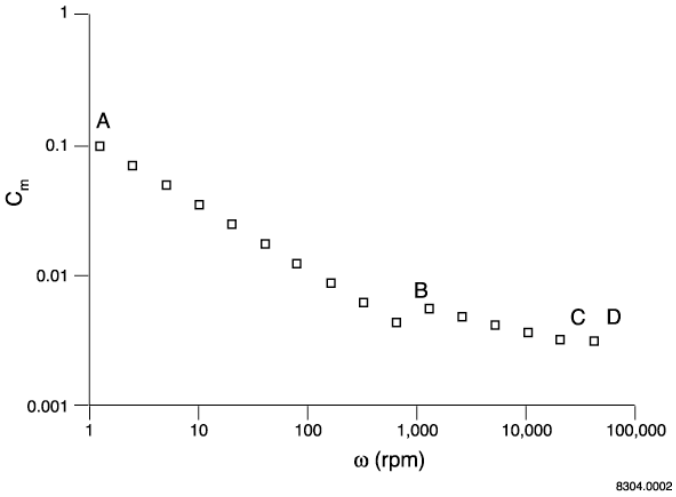

Figure 2. Torque coefficient on end faces of rotor

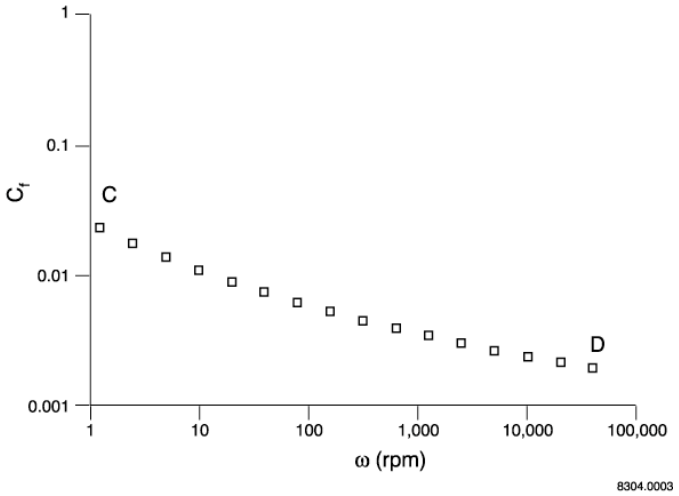

Figure 3. Torque coefficient on cylindrical face of rotor

(turbulent). Clearly, the flow during most of the transient is turbulent or, on the end faces, a combination of turbulent and transition flow. Laminar flow only occurs at low speeds. The large difference between the span of flow regimes for the end faces and the cylindrical face is somewhat surprising.

The angular velocity of the flywheel can be calculated from the equation of motion of the rotor which, after substituting the drag torques from Eq. 1 and 2, is given by

$$I_z \frac{d\omega}{dt} = -2M_1(\omega) - M_2(\omega) \tag{6}$$

where I_z is the polar moment of inertia of the rotor (0.633 kg-m^2). The rate at which energy is removed from the flywheel, or the windage power, is equal to

$$P_w = [2M_1(\omega) + M_2(\omega)]\omega \tag{7}$$

Integration of Eq. 6 yields the flywheel speed as a function of time. The calculated angular velocity of the test rotor is compared with the measured angular velocity in figure 4. Initially, the rate of energy removal by the windage torque is 254 kW. As the flywheel slows, the drag torque decreases. Agreement between the measured data and the results calculated using the torque coefficients given by Eq. 4 and 5 is excellent. The divergence between the calculated and measured rotor speed near the end of the transient is probably due to the fact that the drag forces from the air turbine and bearings were neglected in the calculations. This drag is estimated to be less than 100 W [6]. Although small in comparison to the windage losses in the beginning of the test, these losses can be significant near the end of the

test. Such losses are not important to flywheel safety issues addressed here.

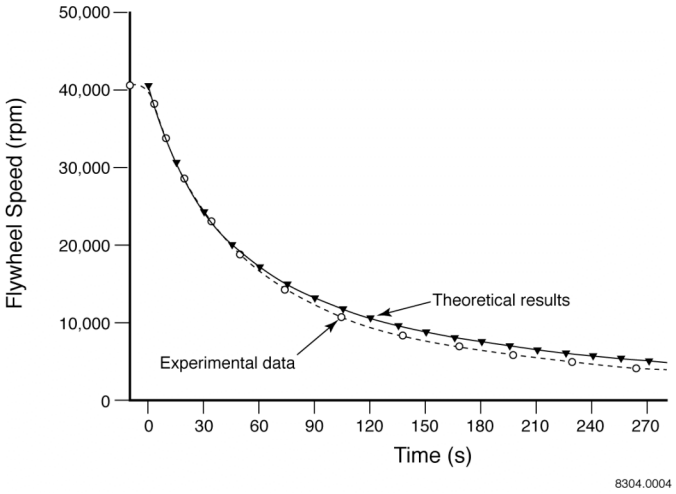

Figure 4. Comparison of measured and calculated flywheel angular velocity during a loss-of-vacuum event

The validity of applying the loss-of-vacuum test data for an unenclosed rotor to the safety assessment of the bus flywheel design depends on whether or not the drag forces are similar in the two systems. The same calculations as those given above can be used to analyze the response of the bus flywheel to a loss-of-vacuum event, with the exceptions that the properties of nitrogen must be replaced by the properties of air and the torque coefficients in Eq. 4 and 5 must be replaced by those for an enclosed rotor. Both the properties and the torque coefficients for this case are also contained in [3]. For convenience, the torque coefficients for the enclosed rotor are summarized in Appendix B of this paper.

Figure 5 compares the calculated responses of the test rotor and the bus rotor under similar loss-of-vacuum conditions. For the purposes of this comparison, the diameter and length of the bus rotor were assumed to be identical to those for the test rotor. The gap dimensions for the bus flywheel, however, were obtained from table 1. The figure indicates that the drag torques in the two systems are similar, with the test conditions being somewhat more severe. Thus, applying the test results to the safety of the bus flywheel is conservative. It is perhaps surprising that the windage losses are greater in the unenclosed system, with the initial energy loss rate in the test equal to 254 kW compared to 156 kW for the bus flywheel geometry; however, Bilgen and Boulos [7] point out that the moment coefficient for drag on a cylinder decreases with increasing gap for low Reynolds numbers, but increases with increasing gap for high Reynolds numbers. At the beginning of a loss-of-vacuum transient, the gas flow inside the flywheel containment is highly turbulent. As time progresses, the Reynolds number decreases. This leads to greater initial drag in the unenclosed system but less drag later in the transient, as indicated in figure 5 by the convergence of the two curves at low speeds.

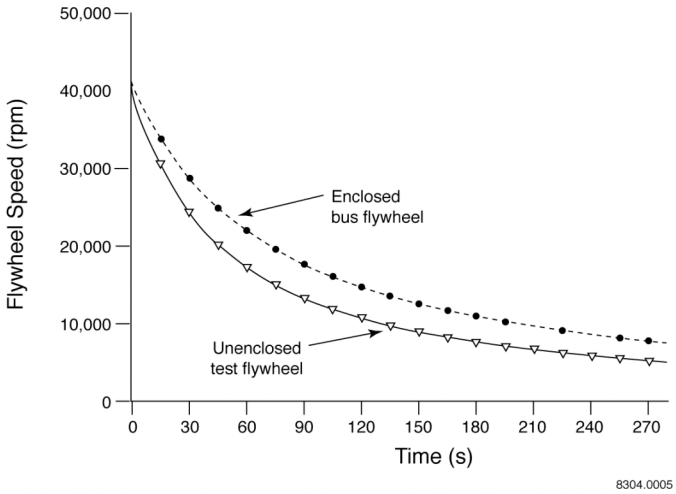

Figure 5. Comparison of bus and test flywheel response

FLYWHEEL SURFACE HEATING

The primary safety concern during a rapid loss-of-vacuum accident is whether or not windage heating on the flywheel surface will damage the composite sufficiently to cause significant material ejection. If the material comes off asymmetrically during failure, the resulting shaking forces could be sufficient to fail the remainder of the rotor or to tear the rotor away from its bearings. On the other hand, if little or no material is lost, or if the material is lost symmetrically, the rotor will remain in balance and the windage forces will help to safely de-energize the flywheel.

Overheating of the composite will only damage the resin, not the graphite fibers. Polymeric resins undergo a gradual softening over a narrow temperature range rather than an abrupt phase transition at a well-defined melting point. The glass transition temperature T_G, that characterizes this softening region, is defined by discontinuities in higher-order derivatives of the thermodynamic functions. The viscosity of the resin decreases by many orders-of-magnitude over the transition region such that, under the centrifugal forces present in a flywheel rotor, it is reasonable to assume that the resin strength is negligible when $T > T_G$. A glass transition temperature of 177°C (350°F) has been assumed for the present analysis, which is typical of the types of resins being used for composite flywheel applications. It is worth noting that T_G generally increases somewhat with increasing heating rate;

however, this effect is usually small (<15°F) and will be neglected here. It should also be noted that even if the resin loses its strength on the outside of the rotor when $T > T_G$, this does not necessarily imply that material will be ejected. A more likely consequence is that the softening will only cause a local relaxation of the radial loads or, at most, a local delamination. Previous tests have shown that delamination in the outer ring of the rotor will not lead to a more serious event before the flywheel can be de-energized.

Most of the heating of the flywheel during a rapid loss-of-vacuum event comes from viscous dissipation in the narrow boundary layer next to the flywheel rim's outer surface. Because the heating is rapid and because the radial conductivity of the composite is low (0.43 W/m-K), it is reasonable to assume that the surface temperature can be calculated using the classical result for frictional heating next to an adiabatic wall. The basis for the derivation (see [8], chapter 9) is the fact that the Prandtl number for many fluids (including nitrogen and air) is approximately equal to one over a wide range of pressures and temperatures. It can then be shown that the surface temperature T_s is related to the temperature T_∞ of the fluid outside the boundary layer by

$$T_s = T_\infty + \frac{1}{2C_p} U^2 \qquad (8)$$

where C_p is the heat capacity of the fluid at constant pressure and, for application to the moving surface of the flywheel geometry, U is the tip velocity, or $U = a\omega = v_a$. This is the same equation as the equation for the stagnation temperature in a stream of velocity U; however, the similarity of the two results is a consequence of the fact that the Prandtl number N_{Pr} is assumed to be one in the derivation of Eq. 8. The Prandtl number is defined by

$$N_{\mathrm{Pr}} = \frac{\mu C_p}{k} \approx 1 \qquad (9)$$

where k is the thermal conductivity of the fluid. Substituting Eq. 9 into Eq. 8 gives the surface temperature in the form

$$T_s = T_\infty + \frac{\mu}{2k} U^2 \qquad (10)$$

which better shows its dependence on the viscous dissipation.

The form of Eq. 8 has also been found to be more generally applicable if a recovery factor r is introduced such that

$$T_s = T_\infty + \frac{r}{2C_p} U^2 \qquad (11)$$

A useful approximation (see [3], section G511.7) that has been used here is that

$$r \cong \sqrt{N_{\mathrm{Pr}}} \qquad (12)$$

for laminar flow and

$$r \cong \sqrt[1/3]{N_{\mathrm{Pr}}} \qquad (13)$$

for turbulent flow. Direct application of Eq. 11, 12, and 13 to the present problem also requires the assumption that the flow in the boundary layer adjusts more rapidly than the flywheel is slowing down. This is the same assumption of quasi-static flow that was used in calculating drag on the flywheel. As in that case, the assumption is reasonable except near the start of the event.

The surface temperature of the flywheel rim during the loss-of-vacuum test was measured using two calibrated infrared probes (OMEGA type K-140 and K-340). One of the probes apparently failed during the course of the test. The trace from the other probe is compared with the calculated temperature in figure 6. Probe calibration was rechecked following the test.

The maximum calculated surface temperature reaches about 393°C (740°F), whereas the maximum temperature indicated by the raw data from the probe was only about 282°C (540°F); however, further inspection of the probe data shows that the apparent surface temperature before and near the end of the test was –29°C (-20°F). This is impossible since the spin pit was initially at room temperature. It is also inconsistent with the reading of the probe that failed, which measured a rotor surface temperature of about 24°C (75°F) prior to pressurization of the system. For these reasons, we believe that the signal from the functioning infrared probe most likely had an offset of 35°C (95°F). This offset probably resided in the data acquisition setup, since post-test calibration of the probe was normal. Fig. 7 shows the measured temperature with the offset applied. Comparison of this curve with the temperature calculated using Eq. 11 through 13 now shows good agreement over most of the transient, except near the beginning where the calculated maximum temperature is 393° (740°F) and the measured maximum temperature, with the offset, is 329°C (625°F).

A preliminary attempt to model this early behavior was made by calculating adiabatic heating of the gas next to the rotor surface as it is accelerated up to the tip velocity of the rotor. The volume of the affected gas was calculated from the length of the rotor and the thickness

of the turbulent boundary layer when it is fully developed (~0.025 m or 1.0 in.). The velocity of the gas and the flywheel during this time can be found from the conservation of angular momentum. From these velocities, the macroscopic kinetic energies of the flywheel and gas layer can be determined. The difference between this energy and the initial kinetic energy of the flywheel is assumed to have been converted irreversibly to heat. The temperature of the gas can then be found from its heat capacity. The calculated initial temperature rise using this model is compared with the data in figure 8. The slope of the calculated temperature is much too great. Apparently, acceleration of the gas in the boundary layer cannot explain the lower peak temperature that was measured. As discussed in the following section, the more likely explanation is absorption of energy by the rotor, which was neglected in the boundary layer calculation.

ESTIMATION OF INTERIOR ROTOR TEMPERATURE

The flywheel surface temperatures at the rim are not the only temperatures of interest. It is also critical to know how much material on the interior of the rotor may have exceeded the glass transition temperature of the resin. Initially, heat flows from the surface to the colder interior;

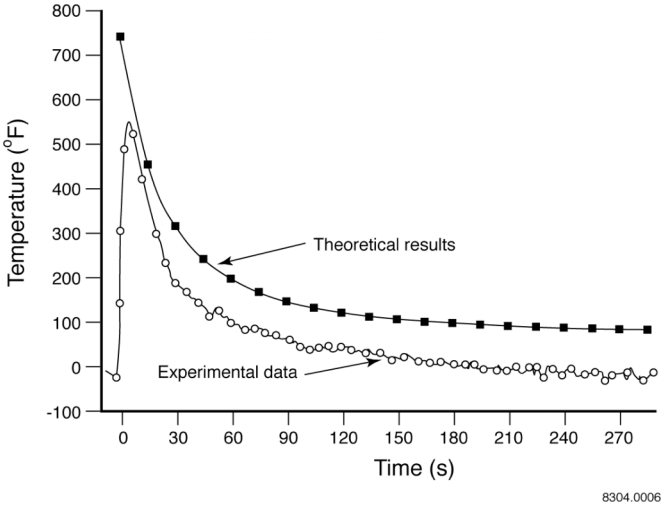

Figure 6. Comparison of calculated and measured flywheel surface temperature

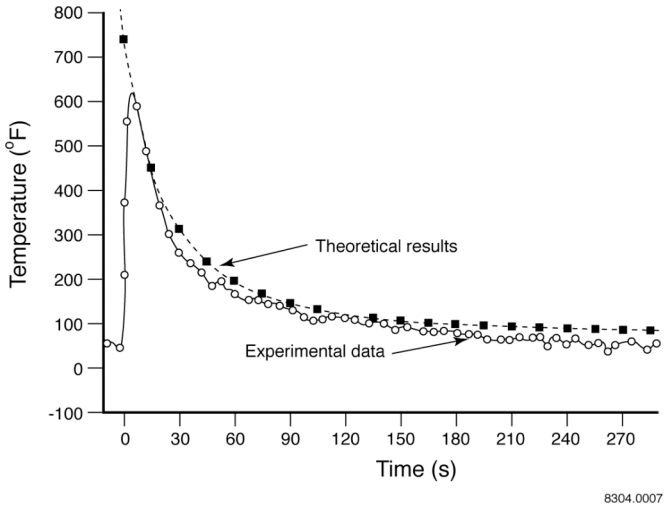

Figure 7. Comparison of calculated flywheel surface temperature with measured temperature shifted to match room temperature prior to the transient

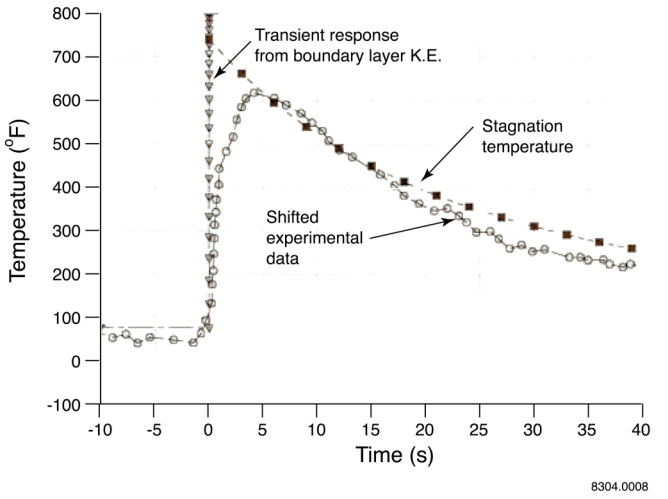

Figure 8. Comparison of calculated and measured flywheel surface temperatures at the beginning of the transient.

however, as time progresses, the surface temperature decreases because the temperature of the boundary layer decreases as the windage forces become smaller. Eventually, penetration of the thermal front reverses and the rotor temperatures everywhere drop below the glass transition temperature.

The only way to capture all of the details of this process is to perform a calculation of the heat transfer in both the solid and the surrounding gas. This requires the use of a sophisticated CFD (computational fluid dynamics) code; however, the calculation would also have to capture the gas flow behavior, since the drag forces and viscous heating depend on the solution of the momentum and continuity equations. Furthermore, unless the calculations are able to accurately reproduce the shear stresses in the boundary layer, they will not be consistent with the experimentally-measured drag coefficients. The turbulent nature of the flow complicates the calculations further because turbulence models have

to be invoked, for which the parameters are not necessarily well known. As a compromise here, we have estimated the subsurface temperatures in the rotor by deriving a calculation of the heat transfer in the rotor with the surface temperatures from the boundary layer model. This is not totally consistent because the boundary layer solution assumed an adiabatic wall; however, as long as the energy being transferred into the rotor is small compared to that being dissipated, the approximation should be valid. The low thermal conductivity of the composite in the radial direction (0.43 W/m-K) makes the assumption plausible.

Calculation of the interior rotor temperatures was performed using the FIDAP Code [9]. The temperature of the cylindrical surface of the rotor was assumed to follow the theoretical result shown in Fig. 6. Furthermore, the temperatures on the top and bottom surfaces were assumed to vary parabolically with radius, as predicted by Eq. 11.

Following pressurization of the vacuum enclosure, the calculated initial temperature on the cylindrical surface of the rotor is 393°C (740°F), which is well above the 177°C (350°F) glass transition temperature. As shown in Fig. 6, the surface temperature decreases as the flywheel slows. Initially, heat flows from the surface to the cooler interior of the rotor. However, as the surface cools, heat transfer is reversed. Eventually, the penetration of the glass transition isotherm stops. The calculations showed that only the outer 2.5 mm (0.1 in.) of the cylindrical surface exceeded the threshold. As might be expected, penetration at the corners was somewhat deeper.

CONCLUSIONS

The rapid-loss-of-vacuum test on a composite flywheel, similar to that planned for an urban bus, indicates that this event is survivable within the test conditions documented in the paper. The test results highlight that this amount of overheating, from a loss-of-vacuum event, did not result in a catastrophic failure, but did structurally degrade the flywheel. The final overspeed test to failure, following the loss-of-vacuum test, revealed about a 15% margin on speed.

Although the test showed that one loss-of-vacuum occurrence is survivable, in practice, that flywheel would be removed from service and replaced with a new unit.

Good correlation exists between the test data and the calculations of the transient speed and thermal profiles in an unenclosed system, representative of a spin test configuration. Applying the appropriate analysis to an enclosed system, representative of the urban transit bus flywheel inside its containment structure, conservatively shows that the power loss profile from windage drag would be less than in the test. This implies that thermal damage from a loss-of-vacuum event in the bus system would also be less severe than that experienced by the test rotor.

REFERENCES

1. J.M. Kramer, R.J. Page, B.J. Hsieh, C.A. Blomquist, and W.C. Lipinski, "Urban Bus Flywheel Interim Safety Assessment," draft report submitted to The University of Texas Center for Electromechanics, May 1996.
2. P.M. Wild, N. Djilali, and G.W. Vickers, "Experimental and computational assessment of windage losses in rotating machinery," ASME Journal of Fluids Engineering, Vol 118, March 1996, pp. 116-122.
3. *The General Electric Data Book on Heat Transfer and Fluid Flow*, Genium Publishing Corporation, Schenectady, N.Y., Revision 74, 1995.
4. P.P. Acarnley, B.C. Mecrow, J.S. Burdess, J.N. Fawcett, P.G. Dickinson, and J.G. Kelly, "A flywheel energy store for road vehicles," 30th International Symposium on Automotive Technology and Automation, Florence, June 1997.
5. *CRC Handbook of Chemistry and Physics*, CRC Press, 76th Edition, 1996, p.6-244.
6. E. Sonnichsen, personal communication, July 1998.
7. E. Bilgen, and R. Boulos, "Functional dependence of torque coefficient of coaxial cylinders on gap width and reynolds numbers," ASME Journal of Fluids Engineering, March 1973, pp. 122-126.
8. V.L. Streeter, Ed., *Handbook of Fluid Dynamics*, McGraw-Hill, 1961.
9. FIDAP Version 7.6, copyrighted by Fluid Dynamics International, Inc., Evanston, Illinois
10. J.W. Daily and R.E. Nece, "Roughness and Chamber Dimension Effects on Induced Flow and Frictional Resistance of Enclosed Cylindrical Discs," MIT Hydrodynamics Laboratory Technial Report No. 27, 1958.

APPENDIX A: EFFECTIVE LEAK DIAMETER FOR A RAPID LOSS OF VACUUM

An estimation of the size of a leak that would be sufficient to cause a rapid containment pressurization can be determined from the equations for the flow of a gas expanding adiabatically from a region of constant ambient pressure and temperature (p_0 and T_0) through an opening of area A into a region of lower pressure p_h . The mass flow rate dm/dt is given by

$$dm/dt = p_0 A \sqrt{\left(\frac{2\gamma}{\gamma-1}\right)\left(\frac{M_w}{RT_0}\right)\left[\left(\frac{p_h}{p_0}\right)^{2/\gamma} - \left(\frac{p_h}{p_0}\right)^{\frac{\gamma+1}{\gamma}}\right]} \quad \text{(A1)}$$

where R is the gas constant and M_w and γ are the molecular weight and specific heat ratio, respectively. The mass flow rate in Eq. A1 increases with increasing pressure difference as long as the velocity is below the sonic velocity. Beyond this point, the flow becomes choked and the mass flow rate is constant. The critical pressure ratio p_{hc}/p_0 below which the flow is choked can be found by determining the maximum flow rate in Eq. A1. The result is

$$\frac{p_{hc}}{p_0} = \left[\frac{2}{\gamma+1}\right]^{\frac{\gamma}{\gamma+1}} \quad \text{(A2)}$$

which, for air, equals 0.528. Substituting this result back into Eq. A1 gives the leak rate for containment pressures less than 0.528 atmospheres as

$$dm/dt = p_0 A \sqrt{\gamma\left(\frac{2}{\gamma+1}\right)^{\frac{\gamma+1}{\gamma-1}}\left(\frac{M_w}{RT_0}\right)} \quad \text{(A3)}$$

Since the windage drag is already significant by the time the containment pressure has reached 0.528 atmospheres, this time is chosen here as the characteristic pressurization time t_p for the loss-of-vacuum event. If the containment pressurization is assumed to be adiabatic, Eq. A3 can be combined with the ideal gas law to give

$$t_p = \frac{p_{hi}V}{dm/dt}\frac{M_w}{RT_0}\left(\left(\frac{p_{hf}}{p_{hi}}\right)^{\frac{1}{\gamma}} - 1\right) \quad \text{(A4)}$$

where V is the free volume inside the containment, p_{hi} is the initial containment pressure and $p_{hf} = 0.528 p_0$ is the final pressure. Substituting the approximate free volume inside the bus flywheel containment (0.009 m^3) into Eq. A4 shows that an equivalent hole diameter of 0.1 mm is sufficient to pressurize the containment in 100 s. According to this analysis, any larger hole would produce a rapid loss-of-vacuum event. In reality, the actual size of the hole would have to be somewhat larger because the above calculations neglected the real geometry of the hole, which would be reflected in a discharge coefficient less than one. The calculation also neglected the effectiveness of the vacuum pump during the event. Nevertheless, the results of the analysis indicate that the leak size does not have to be very large to rapidly pressurize the small free volume inside the containment, especially if the vacuum pump is not effective during this time.

APPENDIX B: MOMENT COEFFICIENTS FOR AN ENCLOSED CYLINDER

The torque coefficients for an enclosed cylinder are also given in [3]. They are repeated here for completeness. The flow regimes and torque coefficients on the end faces of the rotor depend on the Reynolds number and on the spacing ratio s/a. For the bus flywheel geometry given in table 1, the spacing ratios s_t and s_b on both the top and bottom surfaces of the flywheel are equal to 0.11. The correlations selected in [3] were obtained from the work of Dailey and Nece [10] where the torque coefficients for rotating disks were measured. Over the range of gap ratios included in their study (from 0.0127 to 0.217), Dailey and Nece identified the following four different flow regimes (table B1).

Table B1. Flow regimes

Regime I:	Laminar flow with merged boundary layers between the rotor and the containment
Regime II:	Laminar flow with separate boundary layers between the rotor and the containment
Regime III:	Turbulent flow with merged boundary layers between the rotor and the containment
Regime IV:	Turbulent flow with separate boundary layers between the rotor and the containment

Inspection of the dependence of these regimes on the spacing ratio shows that only regimes II and IV exist for a ratio of 0.11. The transition between the two has been calculated here by determining the Reynolds number where the two correlations cross. The boundaries and torque coefficient C_m for the two regimes are given by:

Regime II $N_{\mathrm{Re}} \le 8.27\times10^4$

$$C_m = \frac{1.85\left(\frac{s}{a}\right)^{0.1}}{\left(\frac{\rho\omega a^2}{\mu}\right)^{0.5}} \qquad \text{(B1a)}$$

Regime IV $N_{\mathrm{Re}} > 8.27\times10^4$

$$C_m = \frac{0.051\left(\frac{s}{a}\right)^{0.1}}{\left(\frac{\rho\omega a^2}{\mu}\right)^{0.5}} \qquad \text{(B1b)}$$

The torque coefficient C_f on the cylindrical face of the rotor is somewhat more complicated because of the existence of Taylor vortices in the narrow gap between the rotor and the containment wall. These vortices occur because of instabilities in Couette flow at high rotational velocities. The onset of the instability is characterized by the Taylor number N_{Ta}, which is defined by

$$N_{Ta} = \left(\frac{\rho\omega ab}{\mu}\right)\left(\frac{b}{a}\right)^{\frac{1}{2}} \qquad \text{(B2)}$$

Vortices begin to appear in the gap when $N_{Ta} > 41$. Because the flow beyond this point is dominated by vortex flow, the torque coefficients are usually written in terms of the Couette Reynolds number, defined by

$$N_{\mathrm{Re}C} = \frac{\rho\omega ab}{\mu} \qquad \text{(B3)}$$

The cylinder torque coefficients and flow regimes given in [3] can then be written as:

Laminar $N_{Ta} < 41$

$$C_f = \frac{2}{N_{\mathrm{Re}C}} \frac{\left(1+\frac{b}{a}\right)^2}{\left(1+0.5\frac{b}{a}\right)} \qquad \text{(B4a)}$$

Transition $41 < N_{Ta} < 63$

$$C_f = \frac{0.11\left(N_{Ta}\right)^{0.854}}{N_{\mathrm{Re}C}} \qquad \text{(B4b)}$$

Vortex $63 < N_{Ta} < N_{TaVT}$

$$C_f = \frac{0.476\left(N_{Ta}\right)^{0.5}}{N_{\mathrm{Re}C}} \qquad \text{(B4c)}$$

Turbulent $N_{Ta} > N_{TaVT}$

$$N_{\mathrm{Re}C} = \exp\left\{\frac{\left(1+\frac{b}{a}\right)}{1.2\sqrt{2C_f\left(1+0.5\frac{b}{a}\right)}} - \ln\left[\frac{\sqrt{\frac{C_f}{2}}}{2\left(1+\frac{b}{a}\right)}\right] - 8.58\right\} \qquad \text{(B4d)}$$

where N_{TaVT} is found from the intersection of Eq. B4c and B4d. For the bus flywheel geometry, the Taylor number at this intersection is equal to 551. It should be noted that the turbulent torque coefficient given by the implicit relationship in Eq. B4d must be calculated by finding the root of the equation.